

In-Situ Monitoring of Product Shrinkage During Injection Molding Using an Optical Sensor

CHARLES L. THOMAS

*Department of Mechanical Engineering
University of Utah
Salt Lake City, Utah 84112*

and

ANTHONY J. BUR

*National Institute of Standards and Technology
Polymers Division
Gaithersburg, Maryland 20899*

We have used an optical fiber sensor for in-situ monitoring of product shrinkage during injection molding. The sensor, consisting of a bundle of optical fibers with a sapphire window at its end, is positioned in the ejector pin channel of the mold so that the sapphire window sits flush with the inside wall of the mold cavity. The optical view with this sensor is through the thickness (3.175 mm) of the molded product. The fiber bundle is divided into light excitation fibers and light collection fibers. Light from a helium neon laser is transmitted to the resin via the excitation fibers and the detected response is light that reflects from any interface at which there is a difference of index of refraction. When the molded product shrinks, it separates from the wall and sapphire window, and establishes the geometry of a Fabry-Perot interferometer. During the molding of polystyrene, polypropylene and polyethylene, we observed optical interference fringes that were generated by the movement of the molded product away from the mold wall and window. By counting fringes, a measurement of shrinkage was made. Sensor behavior is described by a model that takes into account the reflection coefficient at each surface, the change in index of refraction of the resin and the coherence of the excitation light. The model has been used to describe asymmetric product shrinkage.

INTRODUCTION

In previous publications we described an optical fiber sensor which is inserted into the ejector pin channel of a mold using an ejector pin sleeve with a sapphire window at its end (1-4). The view of the resin with this sensor is through the sapphire window which is positioned flush with the wall of the mold cavity as shown in *Fig. 1*. The fiber optic cable consists of a bundle of nineteen 100 μm diameter fibers, seven of which carry light from the source and twelve of which transmit collected light to the detector. Our previous work demonstrated the use of this sensor to measure fluorescence from a temperature sensitive dye that was mixed with the processed resin. The fluorescence measurement yielded information about temperature and solidification (crystallization or glass formation) of the resin (1, 2). Also, we developed models to describe the

sensor behavior in terms of thermal diffusion, viscoelastic relaxation and crystallization kinetics (3, 4).

It is also possible to use the sensor in a non-fluorescence mode by monitoring light transmission through the resin (4, 5). Incident light is transmitted through the resin and is reflected back to the sensor from the opposite face of the mold and from any boundary at which there is a discontinuity in the index of refraction. During the molding cycle, the sensor performs four functions: it detects the instant of mold filling at the sensor site; it monitors crystallization of crystallizable resins; it detects the separation of resin from the mold wall upon shrinkage; and, it monitors resin shrinkage and rate of shrinkage. We have used the sensor in the non-fluorescent mode to monitor injection molding of polypropylene. We observed that the light signal clearly distinguished each of the four functions.

Previous publications of this work have concentrated on sensor detection of crystallization kinetics and resin shrinkage (4-6).

Of particular interest in this paper is the study of sensor behavior when the resin shrinks and separates from the mold wall. The geometry of an interferometer is created at the separation event and optical interference fringes develop as the resin recedes from the mold wall. Our objective is to develop a model that describes sensor behavior in terms of optical interference between light that has reflected from interfaces of the sensor/resin/mold arrangement as shown in Fig. 2. We will analyze sensor data obtained from injection molding of polypropylene, polystyrene, and polyethylene.

EXPERIMENTAL PROCEDURE

The experimental arrangement is shown in Fig. 1. The sensor consists of a sleeved ejector pin fitted with a sapphire window at its end. Functioning as an ejector pin, the sensor with sapphire window is positioned flush with the inside wall of the mold cavity and the sensor views the specimen across its thickness. A bundle of optical fibers is inserted into the sleeve and positioned at the face of the sapphire window. There are nineteen 100 μm diameter, multimode optical fibers in the bundle. The overall diameter of the sensor is 6.35 mm (0.25 inch) by 8 cm long; the size of the window is 3.175 mm (0.125 inch) diameter by 3.175 mm long. The optical fiber bundle is approximately 0.5 mm diameter and is protected by stainless steel sheathing. The fiber bundle is bifurcated into one branch of seven fibers which transmits light from the light source and another branch of 12 fibers which carries light to the detector which is a silicon photodiode. The signal from the photodiode was acquired by the computer at a rate of 250 readings per second. The standard uncertainty of the intensity measurements is $\pm 0.4\%$.

The light source was a helium-neon laser, whose light intensity was stable within $\pm 0.5\%$ over the cycle time of the process and whose wavelength, 632.8 nm,

was stable within $\pm 0.01\%$. After the light traverses the length (1.5 m) of the multi-mode optical fiber used in our sensor, the light loses much of its coherent character. The reduced coherence in the interrogating light beam has significant impact on the sensor behavior, and our model will take this into account.

The molded product was a tensile specimen 16 cm in length by 3.175 mm (1/8") thick. Molding of polypropylene, polystyrene and polyethylene was studied. Polypropylene pellets were obtained from Himont Inc. and had a crystallinity of approximately 50%. Polyethylene, Marlex Tr885 from Phillips Petroleum, was a high density resin with crystallinity of 73%. Polystyrene, PS 525P1, was obtained from Fina Corp. (7).

RESULTS AND DISCUSSION

The functionality of the sensor is a consequence of the optical fiber and sapphire window arrangement at the mold cavity surface which permits several reflections to be measured: from the far surface of the mold, from the receding near surface of the resin, and from the sapphire window surface. As shown in Fig. 2, light exiting the optical fiber follows two principal optical paths: (a) light exits from the window, traverses through the polymer resin, reflects from the opposite wall of the mold, retraces its path through the resin and is collected by the optical sensor; and (b) as the resin cools in the mold, it contracts and separates from the sapphire window or the opposite wall creating a gap between resin and window (or wall) that establishes the geometry of a Fabry-Perot interferometer. In the case of optical path (a), light intensity is diminished by crystallizable resin due to the scattering of light by the growing crystallites. For optical path (b), separation of the mold and polymer surfaces is detected by an abrupt increase in reflected light; this is followed by interference fringes which develop via interfering reflections from the sapphire window and the receding polymer resin surface. By counting fringes as a function of time, shrinkage and rate of shrinkage of the resin product are measured in-situ.

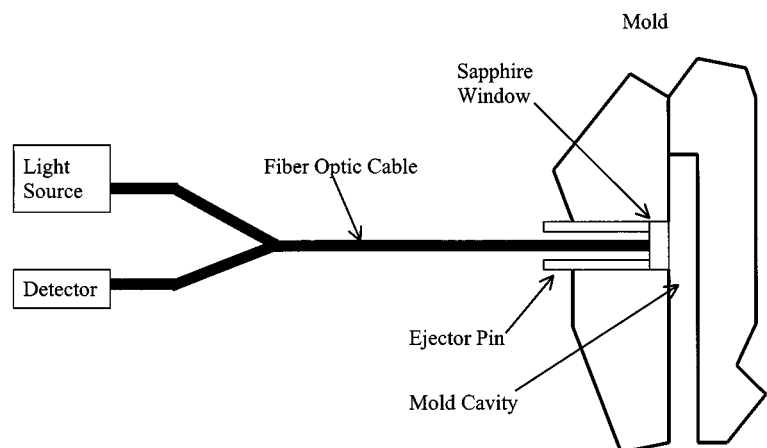


Fig. 1. A schematic of the optical sensor and its connection to the mold, light source and detector is shown.

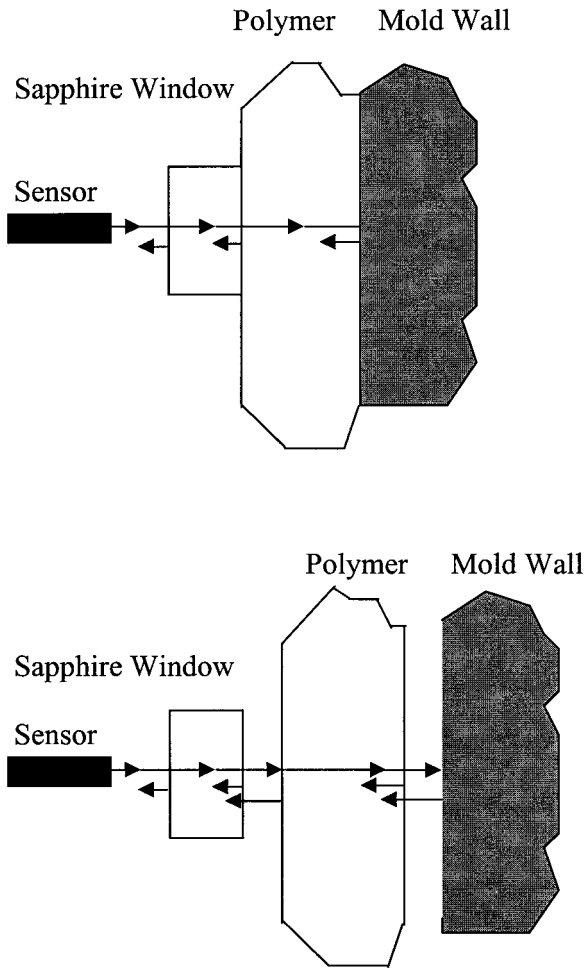


Fig. 2. Reflections of the incident light from each interface of the resin and mold are shown.

The data of Fig. 3 for polypropylene are an example of light detected after traversing optical paths (a) and

(b). Here, light intensity is plotted as a function of time during one injection cycle. The polypropylene resin with an initial temperature of 220°C was injected into the mold whose temperature was held at 38°C by circulating fluid. At $t = 0$ s, the observed intensity is attributed to light which was reflected from the back surface of the empty mold. At $t = 5$ s, the sector of the mold at the optical sensor became filled with resin. Mold filling occurred rapidly, in approximately 0.5 seconds. The initial abrupt decrease in intensity was due to changes in the reflected light from the interfaces: resin/sapphire window and resin/back surface of the mold. The change in slope of the curve at $t \approx 5.5$ s is attributed to the onset of resin crystallization at the surface; attenuation of light due to scattering from the two phase amorphous and crystalline resin began at this time. The approximately linear decrease in light intensity between 6 s and 28 s reflects the growth of microcrystallites in size and number as the interior sectors of the resin cooled below the crystallization temperature. At $t = 32$ s, a distinct and characteristic minimum in transmitted light corresponds to maximum scattered light and is due to the difference in index of refraction between growing crystalline spherulites and amorphous polymer surrounding the spherulite. The phenomenon has been described by Stein and coworkers (8, 9) and was given prominent consideration in the development of our processing model (4).

In Fig. 3, the data from $t = 0$ to $t = 36$ s are from a time period in the mold cycle before polymer shrinkage causes separation between the solidified resin and the mold wall. As long as the resin remains in contact with the wall, we can assume that the product dimensions are constant. The optical consequences of separation between mold and resin are reflections from air/sapphire, air/polymer and air/mold interfaces instead of the resin/mold and resin/window interfaces as diagrammed in Fig. 2. Because the index of refraction differences are greater for the separated interfaces than

Fig. 3. Light intensity versus time for injection molding of polypropylene is shown. The inset contains the fringe pattern immediately after resin/mold separation on an expanded time scale.

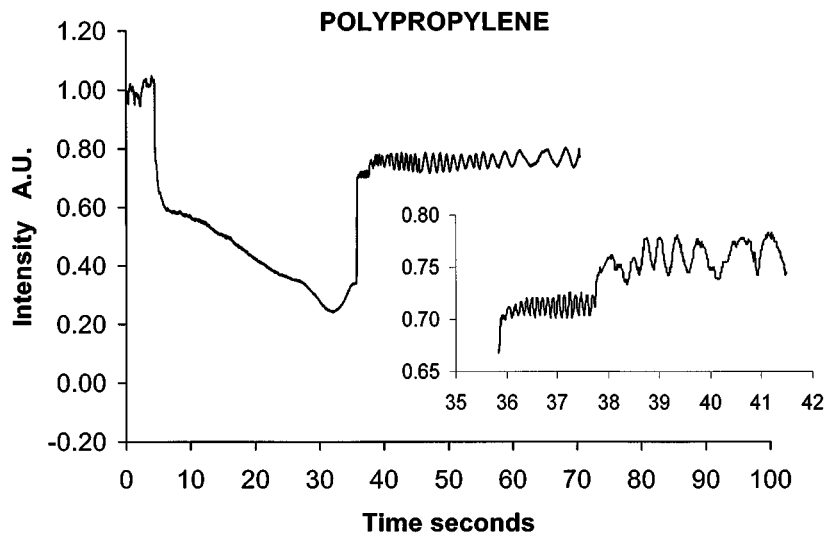
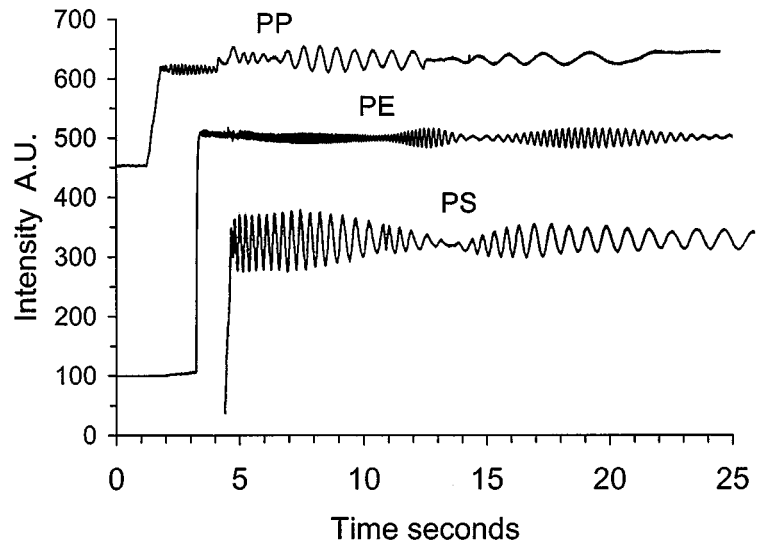


Fig. 4. Interference fringe patterns for polypropylene (PP), polyethylene (PE), and polystyrene (PS) are shown. The polypropylene data are from a different experiment than that shown in Fig. 3.



for sapphire/resin or mold/resin, the reflected intensity is greater. The effect of resin/mold separation is seen in Fig. 3 at $t = 36$ s where a large jump in intensity occurred.

Another distinctive feature of the data of Fig. 3 is the inception of an oscillatory optical signal immediately after separation. The oscillations occur because the separated resin and sapphire window are parallel surfaces that create the geometry of a Fabry-Perot interferometer. Light is reflected from both the window surface and the resin surfaces, and the reflected beams interfere with each other. Since reflection from the surfaces is small, the effect of multiple reflections can be neglected. The inset of Fig. 3 contains the data for $t > 36$ s on an expanded scale. Three fringe patterns are seen: one of small amplitude between $t = 36$ s and $t = 38$ s, a slightly distorted pattern between 38 and 41 s, and a single mode pattern of larger amplitude for $t > 41$ s. We attribute this fringe pattern to the sequential separation of the mold and resin, first from one side of the mold at $t = 36$ s followed by separation from the other side at 38 s.

Figure 4 shows fringe data for polystyrene, polyethylene and polypropylene. We observe that the fringe amplitude fluctuates and there is clear evidence of beats in the oscillations. This was a common observation, although it was not present with every mold cycle. Beating phenomena occur when both product surfaces are separated but are moving at slightly different velocities, thus establishing a modulated interference pattern. If the two velocities are significantly different, greater than 50% different, then the fringe pattern is distorted with secondary and double peaks as seen in Fig. 3 for $38 \text{ s} < t < 41 \text{ s}$. The various fringe patterns that we have observed for all three resins of this study can be interpreted in terms of the relative times of the separation at each side and the velocities of the product surfaces as they move away from the window and wall.

Sensor Model

The detected fringes can be interpreted by using two beam and multiple beam interference theory (10). In general, reflections from all interfaces at which there is a difference in the index of refraction must be considered. Fringes will develop because of the relative movement of the resin surface with respect to the fixed position of the mold wall and window. Figure 5 shows the most general case, i.e. for light transmitting through the resin, reflecting off the back wall, retracing its path through the resin to the detector, and reflecting from all intermediate interfaces. This is the situation for our experiments. The model calculation consists of adding the amplitudes of light waves for each reflection taking into account the appropriate phase of the light wave, the optical path length, the attenuation of light by the resin, the coefficients of reflection, and the phase change which occurs upon reflection.

The total intensity of the five reflected light beams shown in Fig. 5 is

$$I_{tot} = \left[\sum_{i=0}^4 A_i \cos\left(\frac{2\pi}{\lambda}(ct - z_i) + q_i\pi\right) \right]^2 \quad (1)$$

where z_i is the optical path length of the i th light beam, A_i is the amplitude of the electric vector of the i th reflection, λ is the wavelength of light and q_i is 0 or 1 depending upon the phase change at the reflecting interface. The values of A_i will be determined by the reflection/transmission coefficients at the interfaces and by the attenuation due to the crystalline polypropylene. Reflection r at the interface between material with index of refraction n_1 and that with index n_2 is

$$r = \frac{(n_1 - n_2)^2}{(n_1 + n_2)^2} \quad (2)$$

For polypropylene, polystyrene and polyethylene, $n = 1.498, 1.559$ and 1.532 respectively (11–13), and for

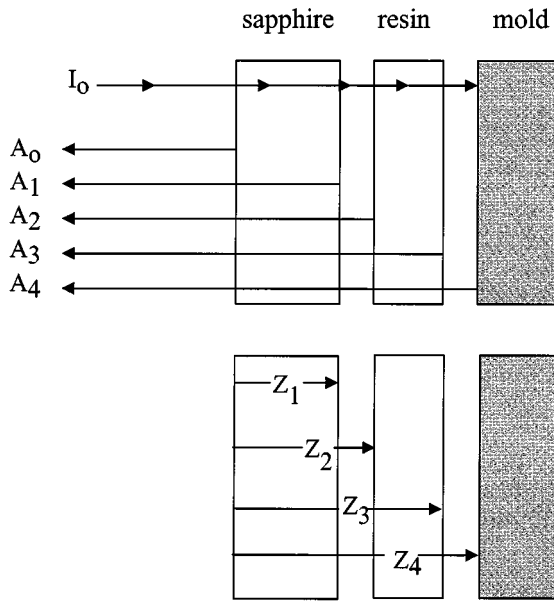


Fig. 5. The electric vector amplitudes \$A_i\$ and the position coordinates \$z_i\$ are shown.

sapphire \$n = 1.760\$. Although these are room temperature values of \$n\$, they will yield close agreement with our reflection observations because the change in \$n\$ between \$25^\circ\text{C}\$ and the temperature at which resin/mold separation occurs, \$60^\circ\text{C}\$ to \$80^\circ\text{C}\$ (3, 4), is less than 0.5%. The reflection coefficient at the steel mold wall was measured and found to be \$0.36 \pm 0.05\$ for steel/air and \$0.16 \pm 0.03\$ for steel/polymer interface. The large uncertainty in these values arises from the difficulty of measuring specular reflections at surfaces that are not optically polished. The attenuation coefficient for transmission through 3.175 mm (1/8 inch) of resin material was measured to be \$0.32 \pm 0.01\$ for 50% crystalline polypropylene, and \$0.33 \pm 0.01\$ for 73% crystalline polyethylene.

The calculation of \$I_{tot}\$ consisted of carrying out the operation on the right hand side of Eq 1 and averaging over time. We obtain cross terms that contain optical path differences, \$z_j - z_i\$, where \$z_i\$ are shown in Fig. 5. Thus,

$$I_{tot} = \sum_{i=0}^4 A_i^2 + 2 \sum_{i,j=0, i \neq j}^4 A_i A_j \cos \left[\frac{4\pi}{\lambda} n(z_j - z_i) + q_{ij}\pi \right] \quad (3)$$

where \$n\$ is the index of refraction of the material in the region \$(z_j - z_i)\$, \$z_i\$ are defined in Fig. 5, and \$q_{ij}\pi\$ accounts for any phase reversal occurring at the interface. For example,

$$I_{12} = 2 A_1 A_2 \cos \left[\frac{4\pi}{\lambda} (z_2 - z_1) + \pi \right] \quad (4)$$

and

$$I_{13} = 2 A_1 A_3 \cos \left[\frac{4\pi}{\lambda} (z_2 - z_1 + n(z_3 - z_2)) \right] \quad (5)$$

where \$n\$ is the index of refraction of the resin.

As the resin shrinks, its density increases causing an increase in \$n\$ thus affecting the optical path length and the reflection coefficients. \$n\$ depends on density through the Lorentz-Lorenz equation,

$$\frac{n^2 - 1}{n^2 + 2} = K\rho \quad (6)$$

where \$K\$ is a constant containing polarizability, molecular weight and Avogadro's number (14). For the model calculation, we assumed that the change in density is inversely proportional to the cube of the shrinkage. Thus,

$$\frac{n^2 - 1}{n^2 + 2} = \frac{n_0^2 - 1}{n_0^2 + 2} \frac{\rho}{\rho_0} = \frac{n_0^2 - 1}{n_0^2 + 2} \frac{(z_3 - z_2)^3}{L_0^3} \quad (7)$$

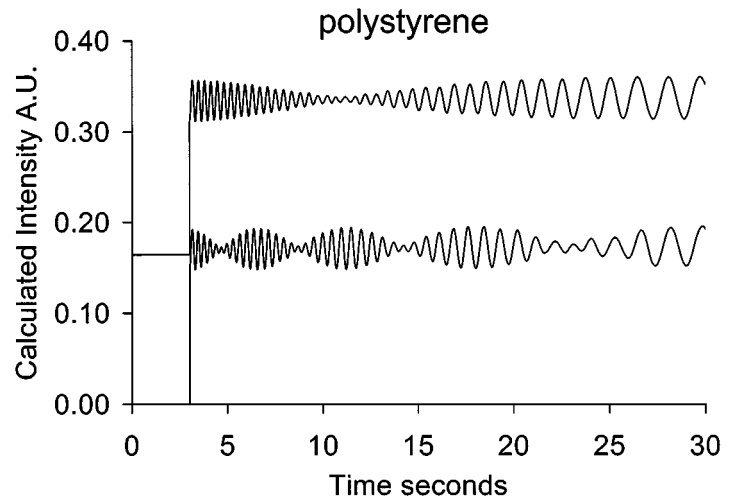
where \$L_0\$ is the thickness of the mold cavity, the shrinkage is \$L_0 - (z_3 - z_2)\$, and \$n_0\$ is the index of refraction at the start of shrinkage. Changes in \$n\$ affect both the optical path through the resin (Eq 5) and the reflection coefficient as expressed in Eq 2. The model calculations will show that changes in \$n\$ can have a large effect on the interferometer fringe pattern, but the absolute value of \$n\$ is of less importance.

Application of Eq 3 to the sensor measurement is greatly simplified because of low coherence in the incident light. The coherence of light exiting the laser is severely compromised while transmitting through the multimode optical fibers of the sensor. The model calculation (see below) supports our assumption that coherence exists only for reflections from near surfaces with optical path differences \$(z_2 - z_1)\$ and \$(z_4 - z_3)\$, i.e. only the cross terms \$I_{12}\$ and \$I_{34}\$ of Eq 3 are considered significant, and all other cross terms are neglected. In addition, the cross term amplitudes, \$A_1 A_2\$ and \$A_3 A_4\$, are reduced by an order of magnitude from those calculated from the reflection coefficients. The model calculation will demonstrate that the lack of coherence works to our advantage. If we include all cross terms, then a very complicated interference pattern results because of the nonlinear dependence of \$n\$ on shrinkage (Eq 7).

Retaining only \$I_{12}\$ and \$I_{34}\$ of the cross terms, Eq 3 reduces to

$$I_{tot} = \sum_{i=0}^4 A_i^2 + 2(A_1 A_2 + A_3 A_4) \cos \left[\frac{2\pi}{\lambda} (L_0 - (z_3 - z_2)) \right] \cos \left[\frac{2\pi}{\lambda} (z_3 + z_2 - 2S_0 - L_0) \right] \quad (8)$$

Fig. 6. Calculated fringe patterns for polystyrene showing beat phenomenon are plotted for front and back surface velocities differing by 2.5% (top) and 10% (bottom).



where S_0 is the thickness of the sapphire window. The argument of the first cosine contains the shrinkage. The argument of the second cosine term is constant if the two surfaces move with the same speed in opposite directions, because z_2 will increase by as much as z_3 decreases. Under these circumstances, the period of Eq 8 is twice that of the period for the simple interferometer with only two separating surfaces. This means that the displacement associated with two adjacent minima in the fringe pattern is λ for Eq 8 rather than $\lambda/2$. The change in period is the result of two interferometers operating in tandem when both surfaces of the resin are separated from the mold. As long as fringes generated by the two interferometers maintain a constant phase relationship, then a simple fringe pattern with λ displacement between fringe minima results. If, however, the velocities $v_2 = dz_2/dt$ and $v_3 = dz_3/dt$ are slightly different in magnitude, then the second cosine term of Eq 8 imposes a beat modulation on the fringe pattern. This is the source of the beating

phenomena that we observed. If the difference in magnitude between v_2 and v_3 becomes larger than 50%, then secondary minima appear, a situation that we have observed occasionally such as in Fig. 3 for t between 38 s and 41 s. Because of the symmetry of the mold dimensions, one would assume that the shrinkage is symmetric and that both surfaces move at the same rate. Our observations indicate that this was only approximately true. When we observed a beating pattern, the velocities of the two surfaces usually differed by no more than 15% when the data were analyzed using Eq 8. On the other hand, if only one side of the resin product separates from the mold, then minima of the resulting fringe pattern will be associated with $\lambda/2$ displacements and no beating pattern will be observed.

For polystyrene, we often observed fringe patterns modulated into beat packets as seen in Fig. 4. To analyze the polystyrene data, the reflection coefficients were calculated using $n = 1.5588$ and we assumed

Fig. 7. The calculated fringe pattern for polystyrene assuming highly coherent incident light is plotted.

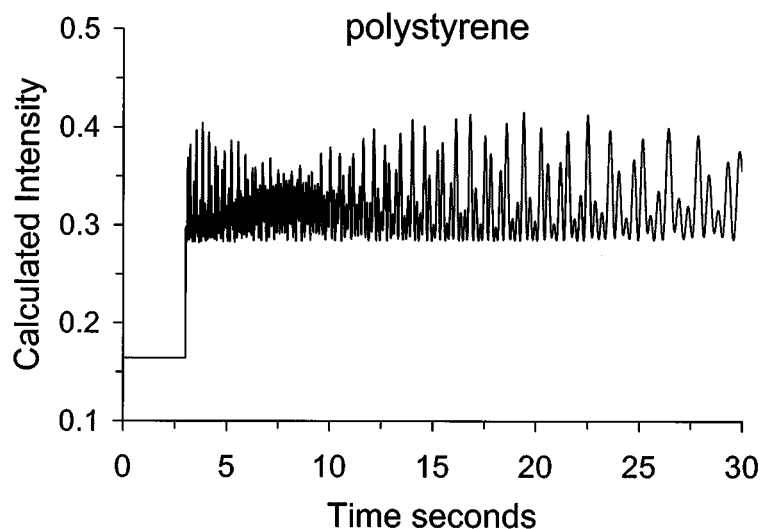
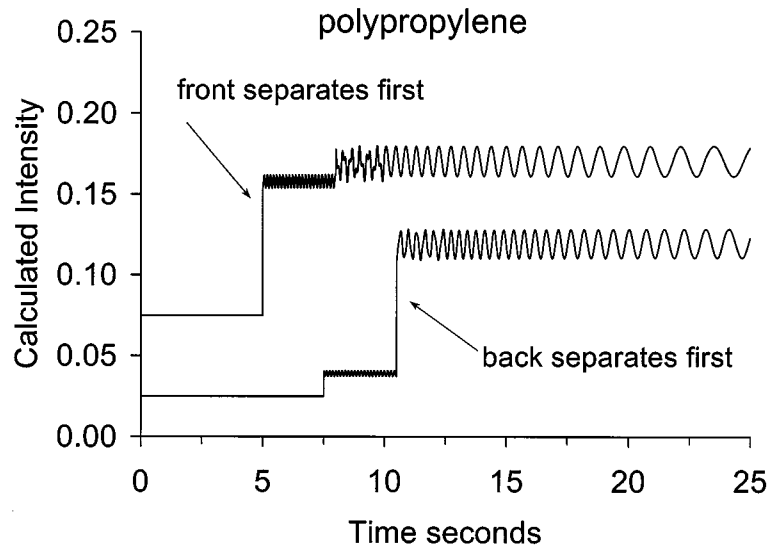


Fig. 8. The calculated fringe patterns for polypropylene are plotted for two conditions: separation from front first and separation from back first.



that light attenuation by polystyrene was zero. During several dozen injection cycles for polystyrene, we did not observe multi-step separation response as we did for polypropylene. Thus, we assumed that both sides separated simultaneously. Application of Eq 8 yields the calculated results shown in Fig. 6 where the calculations were carried out assuming $v_3 = v_0 e^{-t/\tau}$ where $v_0 = -1.0 \mu\text{m/s}$, $\tau = 15 \text{ s}$, and assuming that $v_2 = -1.025v_3$ and $v_2 = -1.1v_3$, i.e. the relative velocities of the two surfaces differ by 2.5% and 10%. The 2.5% relative difference is in close agreement with the observed data of Fig. 4. The calculation for 10% difference (Fig. 6) shows how the beat pattern changes at higher relative velocities. Although not shown here, similar calculations were carried out for polyethylene using $n = 1.532$ and an attenuation of 0.33.

In Fig. 7, we show calculated results for polystyrene when we assume optimum light coherence. This situation permits long range correlations between front and back surfaces of the resin and sapphire window. All cross terms of Eq 3 contribute to the result. The velocities and reflection coefficients were assumed to be the same as those for Fig. 6. The complicated fringe pattern of Fig. 7 results from changes in optical path length in the resin as it shrinks and its density increases. Fringes generated via cross terms involving surfaces on opposite sides of the resin such as z_3-z_0 , z_3-z_1 , etc, do not maintain a fixed phase relationship with fringes generated by z_2-z_1 and z_4-z_3 and therefore are responsible for creating secondary and tertiary minima in the fringe pattern. We see that highly coherent incident light will generate an aggregate signal that is difficult to interpret. None of our observations were similar to the calculated fringe pattern of Fig. 7, and we conclude that long range coherence is not an attribute of this sensor.

To analyze the polypropylene data, we consider the sequential separation of the resin product from front and back surfaces of the mold. For this calculation,

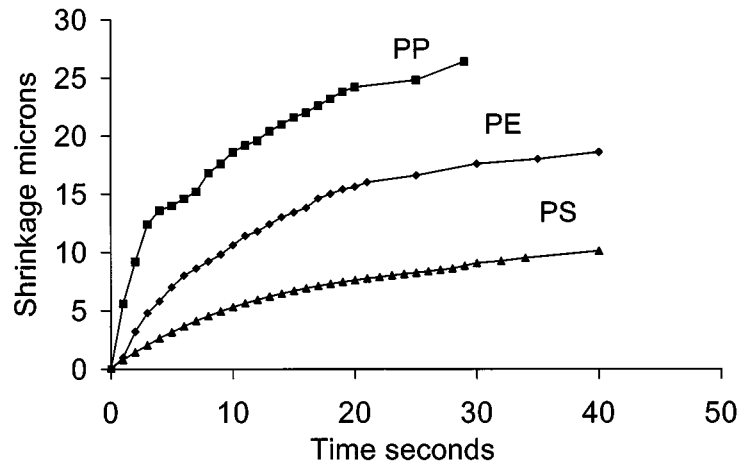
we have attempted to match the observation of Fig. 3 that shows a three step response after separation. We assume that the first separation occurred at the sapphire window at $t = 36 \text{ s}$ followed by separation from the back wall three seconds later. For t between 38 s and 41 s, a mixed fringe pattern was observed for approximately 3 s during which we assume that both surfaces are separated but moving different velocities. At $t = 41 \text{ s}$, a single mode fringe pattern emerged for which we assumed that the two surfaces were moving with the same velocity and the velocity decreased with time. The initial velocity v_2 ($t = 36 \text{ s}$) is set to $2.5 \mu\text{m/s}$ which corresponds to the observed rate of fringe development if we use $\lambda/2$ as the displacement corresponding to adjacent fringe minima. ($\lambda/2$ is used here because only one side is separated.) We use the following set of velocities:

$$\begin{aligned} v_2 &= 2.5 \mu\text{m/s}, & 36 \text{ s} < t < 41 \text{ s} \\ v_3 &= v_0 e^{-t/\tau}, & t > 38 \text{ s} \\ v_2 &= -v_3, & t > 41 \text{ s} \end{aligned} \quad (9)$$

where $v_0 = -1 \mu\text{m/s}$ and $\tau = 10 \text{ s}$. If the two velocities are not equal, then distortion in the fringe pattern occurs as we see from the result for $38 \text{ s} < t < 41 \text{ s}$. For $t > 41 \text{ s}$, the observed pattern is generated from a single mode of movement, in this case calculated by assuming that the $v_2 = -v_3$. The calculated results, shown in Fig. 8, demonstrate the main features of the observation, namely that the product separated from the front surface first followed by back surface separation with the two surfaces moving at different velocities, finally settling into a single mode of shrinkage with both surfaces moving at the same rate. Also, the calculated ratio of intensities before and after separation, 2.20, is in reasonable agreement with our observation of 2.30.

Also shown in Fig. 8 is the calculation for separation first from the back surface followed by front surface separation. The magnitude of the step jumps at

Fig. 9. Measured shrinkage for polyethylene, polystyrene and polypropylene is plotted versus time after separation from the mold.



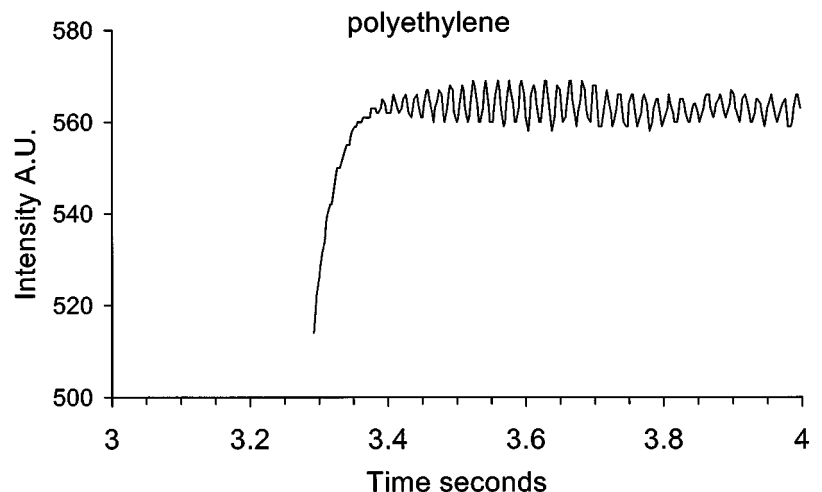
separation does not agree with those observed in Fig. 3. Front surface separation is accompanied by a large change in reflection coefficient relative to that occurring with back surface separation because light from the back surfaces is attenuated by the resin. Front surface separation determines 90% of the jump magnitude. We conclude from the calculations of Fig. 8 that the sequence of events in the data of Fig. 3 is front separation followed by the back separation.

In order to calculate shrinkage, a determination must be made that one or both surfaces have separated from the mold. If only one surface has separated, then $\lambda/2$ is used as the displacement for adjacent fringe minima, but for both surfaces separated, λ is used for the corresponding displacement. The intensity jump upon separation can be used to establish that one or both surfaces are separated as we determined for polypropylene. Also, if the fringe pattern is modulated into beats, then it can be assumed that both surfaces have separated. Using a computer program developed to count the minima of the observed intensities, we carried out measurements of shrinkage

for polyethylene, polystyrene, and polypropylene. Figure 9 shows typical results and shows that the shrink rate of the amorphous polymer, polystyrene, is much smaller than that of the semi-crystalline polymers, polyethylene and polypropylene. Comparison of the absolute shrinkage values is not appropriate because the total shrinkage will be a function of the processing conditions, particularly packing pressure and mold temperature. To date, we have not carried out a systematic study of shrinkage and its relationship to processing parameters.

An evaluation of the uncertainty of the shrinkage measurement is problematic for two reasons: (a) using monochromatic light, an accurate shrinkage measurement depends on confident acquisition of the first fringe, and (b) we must determine that one or both sides have separated in order to assign the appropriate displacement associated with each fringe event. Examining the polypropylene and polystyrene data of Figs. 3 and 4, we find that our acquisition rate is high enough to acquire the first fringe after separation and that the starting point of our fringe count is accurate.

Fig. 10. The polyethylene data of Fig. 4 near the time of separation are shown on an expanded time scale.



The polyethylene data, however, exhibit a problem that is presented in the expanded scale of Fig. 10 where we have zoomed-in on the data at the time of separation. The time of the first fringe event is ambiguous because it appears that, between 3.3 and 3.4 s, there could be a half dozen fringes which are not visible due to a relatively slow acquisition rate. In this case we count fringes from the first visible fringe, but it is understood that the absolute value of shrinkage has an estimated error of five to ten fringes. If we assume that we have accurately acquired the first fringe and that we have determined that one or both sides have separated, then the uncertainty in the shrinkage measurement is conservatively given as $\pm \lambda/2$ or $\pm 0.317 \mu\text{m}$.

An alternate approach to measuring shrinkage is to use a white light interferometer. Using white light for the source, shrinkage is measured by detecting minima in the spectral response, and it is not necessary to count fringes. The relationship between separation d of reflecting surfaces and the wavelengths λ_1 and λ_2 of adjacent minima in the spectrum is

$$d = \frac{\lambda_1 \lambda_2}{2(\lambda_2 - \lambda_1)} \quad (10)$$

In our case, there are two pair of reflecting surfaces in the mold which will yield two pair of minima in the spectrum. A white light interferometer would eliminate ambiguity concerning the first fringe event. Such a device could be implemented using a state-of-the-art spectrograph with an arrayed CCD detector, with which it is possible to obtain spectra over a broad wavelength range in a fraction of a second. Given that shrinkage occurs over a period of tens of seconds, such acquisition rates would be acceptable.

SUMMARY AND CONCLUSIONS

We have demonstrated the operation of an optical fiber sensor that occupies the ejector pin channel of an injection mold. Using a helium neon laser light source, the sensor is used to detect light reflections from the interfaces in the resin filled mold. From these reflections we are able to carry out in-situ detection of mold filling, separation of the resin product from the mold wall, and shrinkage and rate of shrinkage of the molded product. We have shown that resin separation from the mold wall creates the geometry of a Fabry-Perot interferometer and that fringes generated by this interferometer can be used to measure product shrinkage. We have constructed a model with which we describe the prominent features of sensor

response, such as sequential separation from front and back surfaces and the effect of different velocities for front and back surface movement. The model also supports our assumption that long range correlations are absent in the sensor response, i.e. those reflections which derive from opposite sides of the resin product do not produce interference fringes of sufficient magnitude to be detected by the silicon photodiode detector. By counting the fringes, we were able to calculate the shrinkage of injection molded polypropylene, polystyrene and high density polyethylene.

The model has helped us to understand two asymmetric phenomena that we observed with this sensor: sequential separation of resin from the mold walls, and different shrinkage rates for the two surfaces. These effects may indicate non-uniform residual stress distribution in the product and may be used as predictors of warpage in the product. Future work in our laboratory will concentrate on the application of a white light interferometer and on developing relationships between shrinkage, rate of shrinkage, warpage, and processing conditions.

REFERENCES

1. A. J. Bur, F. W. Wang, C. L. Thomas, and J. L. Rose, *Polym. Eng. Sci.*, **34**, 671 (1994).
2. A. J. Bur and C. L. Thomas, *Proc. SPE ANTEC Mtg.*, **40**, 490 (1994).
3. A. J. Bur and C. L. Thomas, *Polym. Eng. Sci.*, **37**, 1430 (1997).
4. C. L. Thomas and A. J. Bur, *Polym. Eng. Sci.*, **39**, 1291 (1999).
5. A. J. Bur and C. L. Thomas, *Proc. SPE ANTEC Mtg.*, **41**, 2798 (1995).
6. A. J. Bur and C. L. Thomas, Method and Apparatus for Monitoring Resin Crystallization and Shrinkage During Polymer Molding, U.S. Patent no. 5,519,211, May 21, 1996.
7. Identification of a commercial product is made only to facilitate experimental reproducibility and to describe adequately the experimental procedure. In no case does it imply endorsement by NIST or imply that it is necessarily the best product for the experiment.
8. R. S. Stein and M. B. Rhodes, *J. Appl. Phys.*, **31**, 1873 (1960).
9. D. Y. Yoon and R. S. Stein, *J. Polym. Sci. Polym. Phys.*, **12**, 735 (1974).
10. P. Hariharan, *Optical Interferometry*, Academic Press, New York (1985).
11. W. B. Westphal and A. Sils, *Dielectric Constant and Loss Data*, U.S. Air Force Materials Laboratory Technical Rept. AFML-TR-72-39 (April 1972).
12. E. M. Amrhein, *Kolloid Z. Z. Polym.*, **216-217**, 38 (1967).
13. D. W. McCall, *Rev. Sci. Instrum.*, **28**, 345 (1957).
14. C. P. Smyth, *Dielectric Behavior and Structure*, McGraw-Hill, New York (1955).